NUCLEAR ISOTOPE THERMOMETRY

S.R. Souza[a], W.P. Tan, R. Donangelo[a], C.K. Gelbke, W.G. Lynch and M.B. Tsang

We discuss different aspects which could influence temperatures deduced from experimental isotopic yields in the multifragmentation process. It is shown that fluctuations due to the finite size of the system and distortions due to the decay of hot primary fragments conspire to blur the temperature determination in multifragmentation reactions. These facts suggest that caloric curves obtained through isotope thermometers, which were taken as evidence for a first-order phase transition in nuclear matter, should be investigated very carefully.

1. Underlying assumptions

For studies in the multifragmentation process temperatures were extracted from the isotopic abundances, using the isotope thermometry method proposed by Albergo *et al.* [1]. The idea of the method is to determine the double ratios of the yields of four suitably chosen isotopes, (A_1, Z_1), (A_1+1, Z_1), (A_2, Z_2), (A_2+1, Z_2),

$$\frac{Y(A_1,Z_1)/Y(A_1+1,Z_1)}{Y(A_2,Z_2)/Y(A_2+1.Z_2)} = C\exp(\Delta B/T_{iso}) \tag{1}$$

where C is a constant related to spin values and kinematic factors, $\Delta B = B(A_1,Z_1) - B(A_1+1,Z_1) - B(A_2,Z_2) + B(A_2+1,Z_2)$ is obtained from the binding energies of the isotopes, and T_{iso} stands for the temperature deduced from this isotopic thermometer.

The basic physical hypotheses of the isotope thermometry method are:

1. an equilibrated source is formed after the most violent stages and it decays simultaneously and statistically,
2. all the events of the reaction corresponding to fragments formed at the same temperature,
3. Overall neutron and proton chemical potentials can be defined and therefore cancel out in Eq. (1), and
4. distortions on the isotopic temperature due to secondary decay of hot primary fragments may be neglected.

Although the Statistical Multifragmentation Model [2], used in the discussion below, is based on the first assumption, the last three hypotheses are not supported by the model, as we shall discuss in detail.

The SMM uses the Monte Carlo method and averages observables with the statistical weight over decay partitions. A multifragment decay partition is *defined* in the SMM approach [2] as a specific set of emitted fragments and light particles. For simplicity, each partition in the SMM approach is weighted according to the entropy of the partition. The dominant contribution to this entropy comes from internal phase space of fragments which plays the role of a heat bath just as an excited residue plays the role of a heat bath within compound nuclear decay theory [3].

By applying the energy conservation one obtains a temperature T that describes the internal excitation and translational energies of fragments within a given partition. Even though the overall system is assumed to be in equilibrium at a fixed excitation energy E_0^*, different decay partitions have

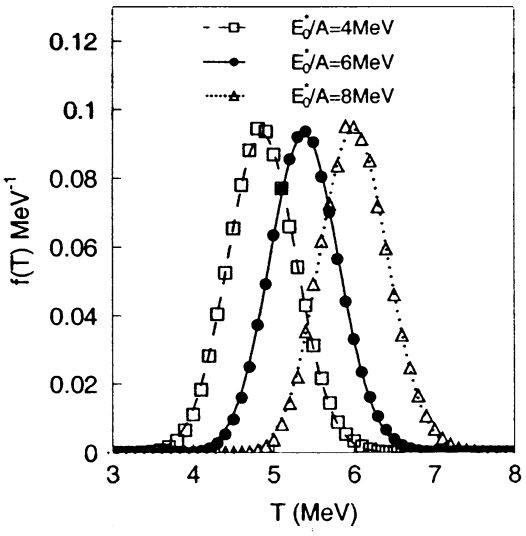

Figure 1: The points denote distributions of temperatures calculated with the SMM approach for the decay of a ^{112}Sn nucleus. The lines denote gaussian fits to the calculated distributions.

different Coulomb, binding, and translational energies and, consequently, different excitation energies of the emitted fragments. Therefore the temperature T of the fragments varies from one decay partition to another, reflecting the differences between the Coulomb, binding and translational energies of the various partitions.

2. Primary Temperatures

The SMM procedure leads to a distribution of the temperatures of the fragmenting system for a given excitation energy in the same sense that the temperature of the daughter nucleus in compound nuclear decay theory varies as a function of the Coulomb barrier and separation energy of each decay channel. Fig. (1) shows the temperature distributions for the fragmentation of an excited ^{112}Sn nucleus at three different excitation energies obtained with the SMM. These distributions are well fitted by gaussian functions with variances σ_T^2 that are fairly independent of the energy, $\sigma_T \approx 0.4$ MeV, in the range $3\,\mathrm{MeV} \leq E_0^*/A \leq 10\,\mathrm{MeV}$.At each excitation energy, we average over all of the partitions and define this average value as the "microcanonical" temperature T_{MIC}.

Since each of the isotopes employed in the thermometer has a specific mass, charge and binding energy, the application of conservation laws sets a constraint on the values available to the remainder of the system. Because of this finite size effect, the temperature distribution obtained when a specific isotope is present is slightly different from the one obtained when all partitions are considered. In particular, a small difference (≤ 0.1 MeV) is observed between the average temperatures for the various isotopes; this is illustrated in Fig. (2) for carbon isotopes from the fragmentation of a ^{112}Sn nucleus at $E_0^*/A = 6$ MeV. Even though the average temperatures are different reflecting the different binding energies of the three isotopes, all these distributions are gaussians with nearly the same variances. We can extract another temperature T_{IMF} by averaging over partitions which contain an Intermediate Mass Fragment (IMF) with $3 \leq Z \leq 10$. It's interesting to note that T_{MIC} can exceed T_{IMF} at low energies by as much as 0.2 MeV, in part because it takes more energy to emit an IMF than to emit an equivalent mass in the form of alpha particles, leaving less energy for thermal excitation.

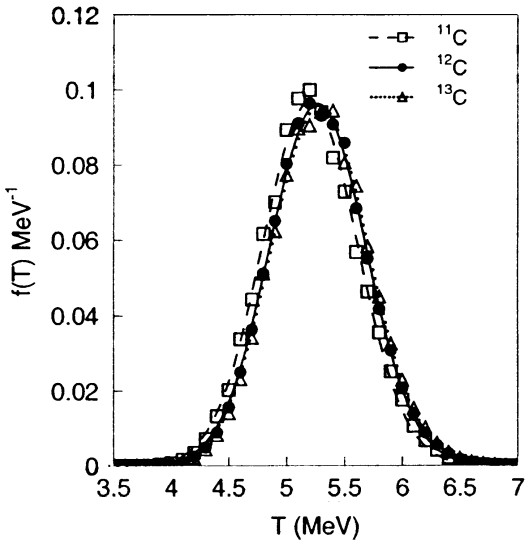

Figure 2: The points denote temperature distributions calculated with the SMM approach for the different isotopes considered in the carbon thermometer. The lines denote gaussian fits to the calculated distributions.

The basic idea contained in Eq. (1) was derived under the assumption that the primary yields are well represented by the grand canonical approximation at a single breakup temperature; the double ratio was invoked to cancel out the contribution to the yields coming from the neutron and proton chemical potentials. In the SMM, however, the temperature varies from partition to partition and the chemical potentials, which appear within the grand canonical formalism as Lagrange multipliers that conserve charge and mass, are not explicitly invoked. Thus, we can not presume the validity of the Albergo's formula (Eq. 1) in the SMM and must test its validity instead.

We begin with a test of the validity of Eq. (1) when one employs the primary yields. The average primary yield for the ground state can be calculated within the SMM and can be used in Eq. (1) to extract isotopic temperatures as follows,

$$\frac{\left\langle N^{gs}_{A1,Z1}\right\rangle / \left\langle N^{gs}_{A1+1,Z1}\right\rangle}{\left\langle N^{gs}_{A2,Z2}\right\rangle / \left\langle N^{gs}_{A2+1,Z2}\right\rangle} = C \exp\left(\frac{\Delta B}{T^{smm}_{iso}}\right) . \tag{2}$$

In previous SMM calculations, experimental binding energies and spin degeneracy factors g^{gs}_{AZ} were used for light nuclei with $A < 5$. Liquid drop binding energies and spin degeneracy factors of unity were used for $A \geq 5$. In this work, we will retain these conventions on spin degeneracy factors so as to be consistent with prior calculations, but we will use empirical binding energies for all nuclei.

In Fig. (3), the isotopic temperatures T^{smm}_{iso} for the carbon thermometer (Z1=Z2=6, A1=11, A2=12) are plotted as the stars for the multifragmentation of a ^{112}Sn source at excitation energies $E^*_0/A = 3 - 10$ MeV. For comparisons, the corresponding T_{MIC} and T_{IMF} for the same system are also shown in Fig. (3) as the dashed and solid lines, respectively. While supporting the concept of isotopic thermometry, the good agreement between T_{IMF} and T^{smm}_{iso} is somewhat surprising, given the strong dependence of the Boltzmann factor on temperature for large ΔB and the width of the temperature distribution shown in Fig. (1). As shown in the following section, it occurs in part due to a large cancellation involving the

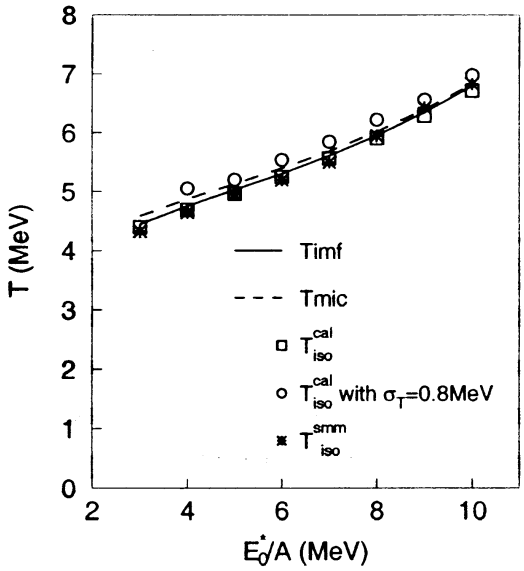

Figure 3: Comparisons of various primary temperatures T_{MIC}, T_{IMF} and T_{iso}^{smm} from the SMM and T_{iso}^{cal} from the analytical calculation in the grand canonical limit. For details see the text.

Boltzmann factor and the temperature dependences of the effective chemical potentials. Fig. (3) also reveals that fairly precise information about T_{IMF} and somewhat less precise information about T_{MIC} is provided by the primary yields. This suggests that given a precise relationship between primary to the final yields, it would be possible to determine the breakup temperature from the measured yields.

3. Effects of Temperature Variations

The surprising consistency between T_{IMF} and T_{iso}^{smm} in Fig. (3) suggests that the corrections to the grand canonical prediction for the isotope temperatures are small, and one may utilize this approach to understand why the temperature variations have so little influence on the results. We take this approach to consider first the influence of the temperature variations and later the consequences of the finite size on the effective chemical potentials.

Considering the influence of the temperature variations in this approximation, we average the grand canonical approximation over the temperature distribution in Fig. (1). Taking this approach, the yield of a particular isotope i in ground state in the framework of Albergo's method [1], when averaged over all possible partitions, becomes:

$$\left\langle Y_i^{gs}\left(T\right)\right\rangle = \int_0^\infty Y_i^{gs}\left(T\right) = Y_i^{gs}\left(\left\langle T\right\rangle\right) \cdot \frac{1}{\sqrt{2p}} \cdot \exp\left[\frac{q^2}{4p}\right] \tag{3}$$

where the corrections to the grand canonical relationship are provided by the correction factor $\frac{1}{\sqrt{2p}} \cdot \exp\left[\frac{q^2}{4p}\right]$ which depends on assumed width σ_T of the temperature distribution, the binding energy of the i-th fragment B_i , the neutron (proton) chemical potentials μ_{NF} (μ_{PF}) and their derivatives through the parameters p and q. These two parameters are defined by

$$p = \frac{1}{2} + \left[\frac{\sigma_T}{\langle T\rangle}\right]^2 \cdot \left[Z_i\alpha_{PF} + N_i\alpha_{NF} + \frac{3}{4} - \frac{B_i}{\langle T\rangle}\right] \quad (4)$$

$$q = \frac{\sigma_T}{\langle T\rangle}\left(Z_i\beta_{PF} + N_i\beta_{NF} + \frac{3}{2} - \frac{B_i}{\langle T\rangle}\right),$$

where

$$\alpha_{PF} = \mu_{PF}^{'}\left(\langle T\rangle\right) - \frac{\mu_{PF}\left(\langle T\rangle\right)}{\langle T\rangle} - \frac{1}{2}\mu_{PF}^{''}\left(\langle T\rangle\right)\langle T\rangle \quad (5)$$

$$\beta_{PF} = \mu_{PF}^{'}\left(\langle T\rangle\right) - \frac{\mu_{PF}\left(\langle T\rangle\right)}{\langle T\rangle}, Similarly for \alpha_{NF} and \beta_{NF}$$

The isotopic temperature can be extracted from the above corrected yields. Replacing $Y(A,Z)$ in Eq. (1) by the right hand side of Eq. (3), one cancels out the spin and mass dependent term C and then obtains:

$$\exp\left[\Delta B/T_{iso}^{cal}\right] = \frac{G(A_1,Z_1)/G(A_1+1,Z_1)}{G(A_2,Z_2)/G(A_2+1,Z_2)}\ , \quad (6)$$

where

$$G(A,Z) = \exp\left[\frac{B_i}{\langle T\rangle} + \frac{\mu_{PF}\left(\langle T\rangle\right)Z + \mu_{NF}\left(\langle T\rangle\right)N}{\langle T\rangle}\right]$$

$$\cdot\frac{1}{\sqrt{2p}}\cdot\exp\left[\frac{q^2}{4p}\right]\ . \quad (7)$$

In the above double ratio the terms involving the chemical potentials evaluated at the average temperature cancel; however, terms in the correction factor involving the derivatives of the chemical potentials remain.

Quantitative estimates of the correction factor require one to obtain estimates for the effective chemical potentials and their derivatives with respect to temperature. The proton and neutron chemical potentials at temperature T may be calculated from the free proton and neutron multiplicities via the expression:

$$\mu_{PF}(T) = T\log\left[\frac{\lambda_T^3 Y_{PF}(T)}{g_{PF}V}\right],\ similarly for \mu_{NF}(T) \quad (8)$$

where $g_{PF}(g_{NF})$ represents the spin degeneracy factor of the proton(neutron). For the calculations presented in this work, it has proven advantageous and reasonably accurate to approximate the yields

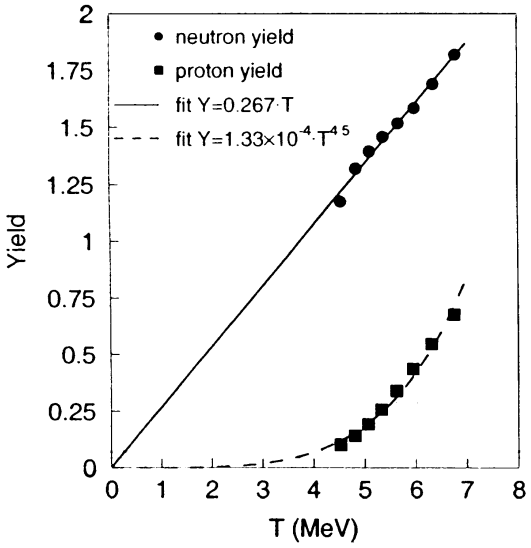

Figure 4: The solid squares and circles denote the free proton and neutron yields, respectively, calculated via the SMM approach. The solid and dashed lines denote fits to the calculated yields following Eq. (9).

$Y_{PF}(T)$ and $Y_{NF}(T)$ over a modest range in temperature by power law expressions in the temperature. In this approximation,

$$Y_{PF}(T) = c_{PF}T^{\gamma_{PF}}\,,\ similarly for Y_{NF}(T) \tag{9}$$

For the decay of ^{112}Sn nuclei at temperatures ranging over $4 \leq T \leq 7MeV$, Y_{PF} and Y_{NF} are well described by $\gamma_{PF} = 4.5$ and $\gamma_{NF} = 1.0$ ($c_{PF} = 1.33 \times 10^{-4}$ and $c_{NF} = 0.267$) according to the SMM; comparisons of this parameterization to yields calculated with the SMM model are shown Fig. (4). These values depend on the density, which has been chosen to be one third that of the saturation density of nuclear matter. Larger values of the free nucleon yields are obtained at lower density.

Using this approximation, the explicit forms of the correction factors in Eqs. (3)-(5) become $2\alpha_{PF} = \beta_{PF} = \left(\gamma_{PF} - \frac{3}{2}\right) = 3$ and $2\alpha_{NF} = \beta_{NF} = \left(\gamma_{NF} - \frac{3}{2}\right) = -\frac{1}{2}$. We note that the correction factor to the temperature T_{iso}^{cal} in Eq. (6) depends on the power law exponents $\gamma_{PF}(\gamma_{NF})$ and not on the absolute values of the proton(neutron) yields.

Due to a strong cancelation between the contributions from the chemical potentials and binding energy factors in the expressions for p and q., the correction factor is of order unity. Values in the range of $\frac{1}{\sqrt{2p}} \cdot \exp\left[\frac{q^2}{4p}\right] \approx 1 - 2$ are obtained, for example, in the decay of ^{112}Sn nuclei at temperatures in the range of $4 \leq T \leq 7MeV$.

The isotopic temperatures T_{iso}^{cal} calculated from Eq. (6) for carbon thermometer are shown in Fig. (3) in comparisons with temperatures T_{MIC}, T_{IMF} and T_{iso}^{smm} derived from the SMM in the previous session. The very good agreement between T_{iso}^{cal} , T_{iso}^{smm} and T_{IMF} indicates that the corrections to the isotopic temperatures associated with these temperature variations are small, although the yields can change by as much as a factor of two. This comparative insensitivity arises because the isotopic thermometers depend logarithmically on the yields.

4. Chemical Potentials

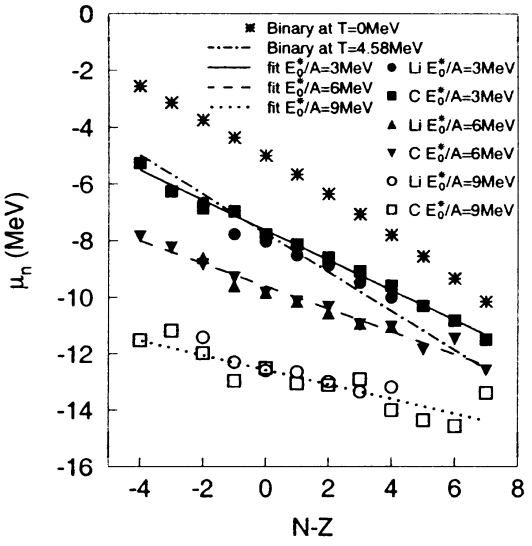

Figure 5: The squares, circles and triangles denote neutron chemical potentials derived from Eq. (10) using SMM predictions for Carbon and Lithium isotopic yields. The stars and the dot-dashed line denote approximate values calculated from Eq.(12) for T=0 and 4.58 MeV, respectively.

The grand canonical limit has a great advantage of providing a simple analytic expression for the isotopic yields from which other useful expressions can be derived. However, the concept of uniform chemical potentials is not a prediction of microcanonical models and must be investigated to determine its applicability to finite systems. We do this by trying to comparing the grand canonical expression for the isotopic yields to the predictions of microcanonical calculations. Using a pair of adjacent isotopes, we invert the grand canonical expression for the isotopic yields of two adjacent isotopes to obtain an equation for the *effective* neutron chemical potential:

$$\mu_n^{eff}(A,Z) = T\log[\frac{g_{AZ}^{gs}}{g_{A+1Z}^{gs}}\left(\frac{A}{A+1}\right)^{3/2} \exp\left(\left(B_{AZ}-B_{A+1Z}\right)/T\right)\frac{Y_{A+1Z}^{gs}}{Y_{AZ}^{gs}}] \quad (10)$$

where g_{AZ}^{gs}, B_{AZ} and Y_{AZ}^{gs} are the ground state spin degeneracy, the binding energy and the ground state primary yield for a fragment with (A,Z), respectively. If the Y_{AZ}^{gs} taken to be the ground state yields predicted by the SMM, $\mu_n^{eff}(A,Z)$ becomes an effective "SMM" chemical potential. By performing SMM calculations, we find the temperature- and isotopic- dependences of the effective neutron chemical potentials given in Fig. (5) for Carbon and Lithium isotopes from the decay of a ^{112}Sn nucleus at excitation energies of $E_0^*/A = 3, 6, 9\ MeV$.

These effective chemical potentials are essentially the same for the Carbon and Lithium isotope chains. This insensitivity to element number is consistent with the concept of a chemical potential and offers support for the use of the grand canonical expression to describe isotopic distributions. There is a dependence on the neutron number of the isotope, however, that lies outside of the grand canonical

approximation. This variation in the neutron chemical potential basically comes as a result of mass, charge and energy conservation for a finite-size system. We can understand the influence of these conservation laws most easily at low excitation energies, where the two largest fragments in the final state are the IMF (Carbon or Lithium in this case) and a heavy residue which contains most of the remaining charge and mass. We estimate the influence of conservation laws at low excitation energy qualitatively by considering binary decay configurations. Assuming that a parent nucleus (A_0, Z_0) decays into a light fragment (A,Z) and a heavy residue $(A_0 - A, Z_0 - Z)$, we can approximate the yield of fragment (A,Z) in its ground state by

$$Y_{AZ}^{gs} \qquad \rho^{gs}\,(A,Z)\,\rho^{*}\,(A_0 - A, Z_0 - Z)\,\overline{\rho}_{REL} \qquad (11)$$
$$g_{AZ}^{gs} \cdot \exp\left[S^{*}\,(A_0 - A, Z_0 - Z)\right]$$
$$\cdot \left[\frac{A \cdot (A_0 - A)}{A_0}\right]^{3/2} \frac{1}{\lambda_T^3}$$

where $\rho^{gs} = g_{AZ}^{gs}$, ρ^{*} and S^{*} are the density of states for the light nucleus in its ground state level, the density of states and entropy of the heavy residue in its excited state, respectively, The other factor, $\overline{\rho}_{REL}\left[\frac{A\cdot(A_0-A)}{A_0}\right]^{3/2}\lambda_T^{-3}$, is the thermal average of the state density of relative motion.

Replacing the yields in Eq.(10) with Eq.(11) and assuming $A << A_0$, One consequently obtains the following expression for the effective chemical potential:

$$\mu_n = -s_n(A_0 - A, Z_0 - Z) + f^{*}. \qquad (12)$$

where the neutron separation energy,

$$s_n(A_0 - A, Z_0 - Z) = B_{A_0 - A, Z_0 - Z} - B_{A_0 - A - 1, Z_0 - Z} \qquad (13)$$

and the reduced free excitation energy has been approximated by its low energy limit,

$$f^{*} = -\frac{T^2}{\varepsilon_0}, \quad \varepsilon_0 = 8MeV. \qquad (14)$$

For the decay ^{112}Sn$\longrightarrow ^{12}$C+X , the chemical potential at $T = 0$, i.e., $-s_n(A_0 - A, Z_0 - Z)$, is plotted as the stars in Fig.(5); the binding energies for these calculations were calculated using the liquid-drop parametrization in ref.[4]. The reduced free energy f^{*} gives a reasonable estimate for the trend with excitation energy. The dot-dashed line in Fig.(5) gives the chemical potential predicted from Eq. (12) for $E_0^{*}/A = 3\ MeV$ $(T = 4.58MeV)$. The predicted trend is close to that predicted by the SMM model (solid circles and squares) but has a somewhat stronger dependence on $N - Z$.

In general, the slope of the effective neutron chemical potential is getting slightly flatter as the excitation energy or temperature increases. If we consider that the system undergoes a multiple fragment decay at higher temperatures, it is clear that approximating the entropy of the remaining system by that of a residue of comparable mass becomes rather inaccurate. The constraints imposed on the total system

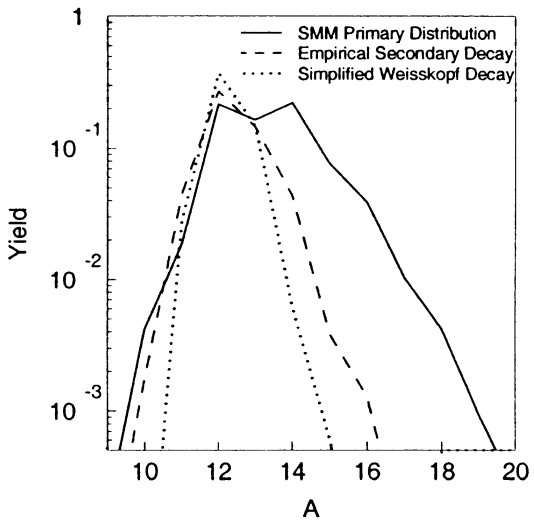

Figure 6: Primary (solid line) and final Carbon isotopic distributions calculated for the decay of the nucleus ^{112}Sn using (dashed line) and neglecting (dotted line) the empirical nuclear structure information in the secondary decay process.

by the isospin asymmetry of one observed fragment should, in that case, be less significant. While there is a mass dependence to the effective chemical potential that is inconsistent with the grand canonical approach, it is useful to note that the mass dependence of the chemical potential (for these systems of more than 100 nucleons) is small if one is mainly concerned with nuclei near the valley of stability. If one cancels the chemical potential effects by constructing double ratios like that of the Algergo formula, the consequence of such finite size effects becomes negligible indeed.

5. Influence of Secondary Decay

Recent works (see for example [5, 6, 7]) qualitatively agree on the point that the isotopic temperature is lower than the thermodynamical one due to the effects of secondary decay. At the quantitative level, details of the population and decay of the excited fragments are important. One issue concerns the importance of utilizing empirical binding energies, energy levels and decay branching ratios for the excited fragments.

Fig. (6) shows the primary and secondary carbon isotopic distributions for the decay of a ^{112}Sn nucleus at initial excitation energies of $E_0^*/A = 4\ MeV$ and $6\ MeV$. The primary distribution (solid lines) is calculated by considering empirical binding energies within the SMM for hot fragments. The simplified Weisskopf evaporative decay procedure of ref. [8] is used for one final distribution (dotted lines). The other final distribution (dashed lines) is obtained by calculating the secondary decay for $Z \leq 10$ hot fragments, as in ref. [7, 9], according to empirical nuclear structure information regarding the excitation energies, spins, isospins and decay branching ratios where available. For hot fragments with $Z \leq 10$ where such information is not available, the decay is calculated according to the Hauser-Feshbach formalism[10]. The contributions to this latter calculation from the secondary decay of hot fragments with $Z > 10$, are calculated, for simplicity, via the secondary evaporative decay procedure of ref. [8]. Decays of fragments with $Z > 10$ make a 15% contribution to the yields of ^{12}C isotopes that may be altered when the decay of hot fragments with $Z > 10$ is calculated more accurately.

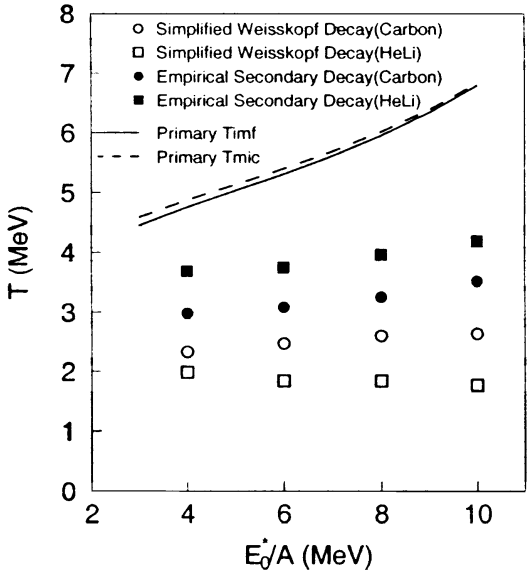

Figure 7: Isotopic temperatures for Carbon and He-Li thermometers calculated with the SMM model using (solid symbols) and neglecting (open symbols) the empirical nuclear structure information in the secondary decay process. The lines are the same as those shown in Fig. (3).

Obviously, in Fig. (6), the final distribution after the empirical secondary decay is much wider than the final distribution obtained via the evaporative decay approach of ref. [8]. This points out the importance of using the empirical information in such calculations. This also leads to the extraction of larger isotopic temperatures via Eq. (1) for the empirical approach. Temperatures for the Carbon isotope thermometer and He-Li thermometer calculated for the two secondary decay approaches are shown, for example, in Fig. (7) for the multifragmentation of a ^{112}Sn nucleus at $E_0^*/A = 4 - 10$ MeV. For reference, the curves T_{MIC} and T_{IMF} from Fig. (3) are also shown as the dashed and solid lines in the figure. Clearly, incorporating empirical information in the decay makes a significant difference. Both calculations provide lower isotopic temperatures than have been obtained in recent experiments.

It should be noted, however, that the simplified Weisskopf evaporative decay, shown in Figs. (6) and (7), is only used in the SMM code of ref. [8] to calculate the decay of fragments with $A > 16$. The decay of lighter fragments is calculated via a "Fermi Breakup" multiparticle decay formalism. This latter decay mechanism makes the dominant contribution to the isotope temperatures calculated via the latter SMM code in ref. [11]. Investigations of the experimental and theoretical basis for the "Fermi Breakup" approach are needed, but are out of the scope of the present work.

Regardless of the decay formalism, memory of the breakup stage is lost via the secondary decay mechanism. The degree of memory loss depends on the details of the secondary decay correction and on the role of short-lived higher lying particle unbound states. A smaller degree of memory loss ensues in models such as those of refs. [12, 13, 14], where few, if any, particle unbound states are considered. The approach of ref. [8] represents the other extreme, wherein all states are considered regardless of lifetime. This issue clearly needs further study to see whether the role of particle unstable nuclei can be constrained, for example, by direct measurements using techniques discussed in refs. [9, 15] or by other experimental observables.

a. Instituto de Fisica, Universidade Federal do Rio de Janeiro

References

1. S. Albergo, S. Costa, E. Costanzo, and A Rubbino, Nuovo Cimento bf 89, 1 (1985).
2. J.P. Bondorf, R.Donangelo, I.N. Mishustin, C.J. Pethick, H. Schulz, and K. Sneppen, Nucl. Phys. A bf 443, 321 (1985); it ibid Abf 444, 460 (1985); it ibid Abf 448, 753 (1986).
3. W. A. Friedman and W. G. Lynch, Phys. Rev. C bf 28, 950 (1983).
4. K. Sneppen, Nucl. Phys. A bf 470, 213 (1987).
5. H. Xi, W.G. Lynch, M.B. Tsang, and W.A. Friedman, Phys. Rev. C bf 54, 2163 (1996).
6. J.P. Bondorf, A.S. Botvina, and I.N. Mishustin, Phys. Rev. C bf 58, 27 (1998).
7. H. Xi, W.G. Lynch, M.B. Tsang, W.A. Friedman, and M. Durand, Phys. Rev. C bf 59, 1567 (1999).
8. A.S. Botvina, A.S. Iljinov, I.N. Mishustin, J.P. Bondorf, R. Donangelo, and K. Sneppen, Nucl. Phys. Abf 475, 663(1987).
9. T.K. Nayak, T. Murakami, W.G. Lynch, K. Swartz, D.J. Fields, C.K. Gelbke, Y.D. Kim, J. Pochodzalla, M.B. Tsang, H.M. Xu, F. Zhu, and K. Kwiatkowski, Phys. Rev. C bf 45, (1992) 132.
10. W. Hauser and H. Feshbach, Phys. Rev. bf 87, 366 (1952).
11. U. Lynen, et al Nucl. Phys. A bf 630, 176 (1998).
12. D.H.E. Gross, Phys. Rep. bf 279, 119 (1997).
13. Pan, J. and S. Das Gupta, Phys. Lett. B bf 344, 29(1995).
14. William A. Friedman, Phys. Rev. C bf 42, 667 (1990).
15. N. Marie, et al Phys. Rev. C bf 58, 256 (1998).